

# Experimental and kinetic modeling study on the gas-phase pyrolysis of hydroxycinnamaldehyde model compounds

*Liang Li<sup>1</sup>, Ruben Van de Vijver<sup>1</sup>, Andreas Eschenbacher<sup>1</sup>, Florence H. Vermeire<sup>1</sup>, Kevin M. Van Geem<sup>1\*</sup>*

<sup>1</sup>Laboratory for Chemical Technology, Ghent University

Technologiepark 125, 9052 Ghent, Belgium

[Kevin.VanGeem@UGent.be](mailto:Kevin.VanGeem@UGent.be)

## Abstract

Hydroxycinnamaldehyde monomers are major pyrolysis products of lignocellulose biomass, and important intermediates in lignin biosynthesis. In this work, for the first time, the gas-phase pyrolysis of two hydroxycinnamaldehyde monomers, *p*-coumaraldehyde (PA) and coniferaldehyde (CoA), was studied experimentally and theoretically at 873–1123 K and 723–923 K, respectively. The experimental data were gathered using a tandem pyrolysis reactor hyphenated with a GC × GC-FID/TOF-MS and a customized GC for on-line analysis. This allowed to quantify polyaromatic compounds with up to four aromatic rings. The potential energy surface calculations at CBS-QB3 level helped to identify a new decomposition path of primary phenoxy-type radicals in PA and CoA pyrolysis, causing the decarbonylation of side-chain (-CH=CHCHO) via a combination of trans-cis isomerization and H-atom migration. This new pathway is essential to predict the conversion of the reactants and the major product yields accurately. It is thus essential that similar pathways should be explicitly accounted for in all future first principles based models that are developed for lignin pyrolysis and oxidation.

## Keywords

Gas-phase pyrolysis; *P*-coumaraldehyde; Coniferaldehyde; Kinetic modeling; Phenoxy-type radicals

## 1. Introduction

Fast pyrolysis of lignocellulosic biomass is potentially one of the most economical routes toward renewable biofuels or high-value chemicals, and its application has gained a large industrial interest<sup>(1–4)</sup>. With this in mind, it is crucial to develop a deeper understanding of the occurring chemical reactions during biomass pyrolysis to steer and optimize these pyrolysis-based

conversion processes, in particular for lignin, as one of the three main components of biomass (5,6).

Lignin is a three-dimensional branched polyphenolic polymer bio-synthesized from three monomeric units (monolignols): *p*-coumaryl alcohol, coniferyl alcohol and sinapyl alcohol that are incorporated into a complicated network through ether (C–O) and condensed (C–C) linkages (7). Due to the complexity and heterogeneity of the lignin structure, the model dimers that represent these linkages, especially  $\beta$ -O-4, which is the most important linkage in lignin, have been extensively studied to understand the pyrolytic reactions of lignin (8–11). Two general mechanisms, concerted pericyclic reactions and free-radical reactions that reveal the initial thermal decomposition of these linkages have been proposed, and they are dominant under different pyrolysis conditions (12). In contrast, the pyrolysis of monomers that represent the essential reactive moieties of lignin and an important product group of lignin pyrolysis has been less explored. For the simple phenolic monomers, such as phenol (13–15), anisole (16–18) and guaiacol (19,20), detailed kinetic models consisting of elementary reactions of pyrolysis processes have been developed. These models are seen as a powerful tool to unravel the underlying chemistry of lignin pyrolysis and to understand the effect of process conditions on the yields of various products (21,22). Besides the above mentioned substituents (hydroxyl and methoxy groups) on aromatic rings, side-chains such as propanoid ( $-\text{CH}=\text{CHCH}_2\text{OH}$ ) on aromatic rings, which are a considerable portion of lignin, also play an important role in the observed diversity of the pyrolysis products (23–25). For the hydroxyl and methoxy groups which are adjacently connected to the aromatic ring in guaiacyl-type model compounds, their interactions have been reported such as those that lead to the formation of 2-hydroxybenzaldehyde from 2-methoxyphenoxy radical (26,27). However, the interactions of aromatic substituents and side-chains are hardly

reported, not only because the larger molecules make it more difficult to establish the detailed kinetic models, but also because they are usually further apart in space. For the monomers with both aromatic substituents and side-chains, such as the above-mentioned monolignols, their pyrolysis mechanisms are typically postulated based on the product distribution and chemical intuition. The detailed kinetic models of these monolignols are still not available even though they are known to be important products of lignin pyrolysis<sup>(23,25,28,29)</sup>.

It has been reported that coniferaldehyde (CoA) is a more important product than coniferyl alcohol from the pyrolysis of G-lignin<sup>(30)</sup>. CoA was also reported as a major product in experiments studying the pyrolysis of coniferyl alcohol<sup>(28,29)</sup>. In addition, *p*-coumaraldehyde (PA) and CoA, as the precursors of monolignols, can be largely incorporated into the lignin structure via genetic engineering<sup>(31)</sup>. Recent studies performed in our group have demonstrated that this technology can be used as a potential tool to control the lignin composition of biomass which allows to increase the production of high-value chemicals via fast pyrolysis<sup>(32–34)</sup>.

Therefore, it is essential to study the pyrolysis products and mechanism of PA and CoA.

Our previous work studied the solid-to-gas pyrolysis of PA and CoA in a single pyrolysis reactor, focusing on the competition of reactions in the condensed and gas phase<sup>(35)</sup>. In addition, we had proposed a preliminary kinetic model describing their initial decomposition under the studied conditions. To the best of our knowledge, the gas-phase pyrolysis of PA and CoA has not been investigated previously. This is a crucial aspect for future reactor and process development because it is essential to understand what happens once these components enter the gas phase.

Therefore, we focus specifically on studying the kinetics of gas-phase thermal decomposition of PA and CoA experimentally and theoretically in the present work, and we have investigated the importance of unknown decomposition pathways using ab-initio calculations.

## 2. Materials and methods

### 2.1. Model compounds

The model compounds used in this study are PA (purity  $\geq 98\%$ , CAS: 2538-87-6, Toronto Research Chemicals Inc.) and CoA (purity  $\geq 98\%$ , CAS: 458-36-6, Sigma Aldrich, Inc.). Figure 1 shows their molecular structures, together with the bond dissociation energies (BDEs) within each compound calculated at the CBS-QB3 level of theory in the previous work<sup>(35)</sup>.

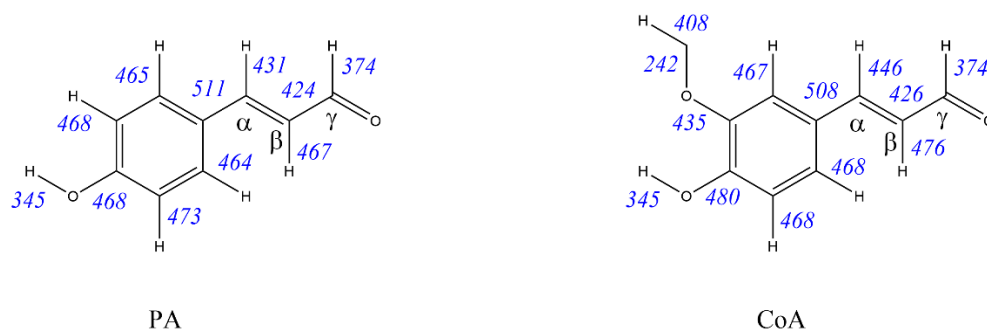


Figure 1. Molecular structures of the model compounds with their corresponding bond dissociation energies (the enthalpy change of the homolysis at 0 K) in kJ/mol calculated at CBS-QB3 level of theory.

### 2.2. Fast pyrolysis and on-line analysis of product vapors

The pyrolysis experiments were performed in a micro-pyrolysis unit consisting of two sections, viz. reactor, and analytics (Figure S1a). The reactor is a tandem  $\mu$ -micro-pyrolyzer (Rx-3050 TR, Frontier Labs, Japan) with two reactors in series. The 1<sup>st</sup> reactor was used to vaporize the solid samples in an externally heated quartz tube with an internal diameter of 4 mm for the initial length of 75 mm, and 2 mm for the remaining length of 45 mm. The 2<sup>nd</sup> reactor was used to study the gas-phase reactions in an externally heated quartz tube (o.d. 6 mm; i.d. 4 mm; L. 120 mm). In this work,  $100 \pm 10$   $\mu\text{g}$  of the sample was loaded in a shallow eco-cup (4 mm height) and inserted into the first reactor via a dropping device. After loading the sample cup to the dropping device, the sample cup was purged for 30 s using the carrier gas (He) and then dropped into the 1<sup>st</sup> reactor where the sample vaporized under the pre-set temperature programs. A carrier gas flow of

210 mL/min was maintained to sweep the sample vapors from the 1<sup>st</sup> reactor to the 2<sup>nd</sup> reactor where the gas-phase pyrolysis happened at a pressure of 3.5 atm. The gas-phase decomposition of PA and CoA were studied in the 2<sup>nd</sup> reactor over the temperature range of 873–1123 K and 723–923 K, respectively, with the residence time of ~ 0.4 s. The interface temperature between the two reactors was set at 623 K, high enough to prevent vapor condensation and low enough to minimize cracking reactions. The calibration curves of each reactant were obtained at 623 K, and only one peak that should be the reactant was observed.

Part (split ratio 100:1) of the effluent from the 2<sup>nd</sup> reactor passed through the GC inlet maintained at 573 K and then entered a guard column. In this work, the GC inlet split ratio was calculated by dividing the column carrier gas flow rate (2.1 mL/min) into the constant flow rate (210 mL/min). The products were firstly trapped with a micro-jet cryo-trap cooled with liquid nitrogen at 77 K. After 5 minutes, the cryo-trap was switched off automatically. The trapped products were released gradually with the increasing oven temperature, which started from 313 K (6 min hold) and then increased to 573 K (2 min hold) at a 5 K/min heating rate. The released effluent was divided into two streams for the simultaneous analysis of permanent gases and water in a customized multicolumn GC, while other products along with unreacted model compounds were analysed in a GC × GC coupled to flame ionization detector (FID) and time-of-flight mass spectrometry (TOF-MS). More details of the analysis section have been described elsewhere <sup>(35)</sup>. The schematic drawing of the 2<sup>nd</sup> reactor with the temperature profiles measured inside the reactor tube is shown in Figure S1b. The process gas temperature was measured at different axial positions by moving a K-type thermocouple inside the reactor using only carrier gas, which provided the actual process gas temperature parameters for the simulation. Prior to the gas-phase thermal decomposition experiments, the temperature program of the 1<sup>st</sup> reactor was optimized to

ensure that the solid samples vaporized at a constant rate and without any residue remaining in the sample cup. This was done by directly connecting the micro-pyrolyzer to the FID via a deactivated guard column (780 mm x 0.25 mm). For this test, the 2<sup>nd</sup> reactor and GC oven temperatures were maintained at 573 K to prevent the condensation of the vapors. The profiles are approximately rectangular (Figure S2), indicating that the applied temperature programs (Table S5) provide an approximately constant feed flow rate to the 2<sup>nd</sup> reactor. The arrow's width represents the vaporization time, 2.25 min for PA and 2.5 min for CoA.

For the pyrolysis tests, a TOF-MS (BenchTOF-Select, Markes International) was connected to identify the products with an ionization voltage of -70 eV, while the FID was used to quantify the product yields. The FID response of the two model compounds used as feed was calibrated by injecting different sample amounts at the temperatures for constant volatilization (Table S5). All other products detected by FID were quantified based on the effective carbon number method<sup>(36)</sup>. Response factors of those gases (H<sub>2</sub>, CO, CH<sub>4</sub>, C<sub>2</sub>H<sub>4</sub>, C<sub>2</sub>H<sub>6</sub> and C<sub>2</sub>H<sub>2</sub>) observed with the customized GC were determined by means of a gaseous C<sub>2</sub>- calibration mixture (Air Liquide, Belgium). The carrier gas helium was excluded for the calculation of product mole fractions. Each experiment was performed two times at the same condition in order to calculate the standard error, which was less than 2.2% for the mole fractions of reactants and major products.

### **2.3. Theoretical calculations and kinetic model construction**

The transition states, thermodynamic properties, and rate coefficients of key reactions were calculated using the high-performance supercomputer of Ghent University at the CBS-QB3 level as implemented in Gaussian 16<sup>(37)</sup>. For species and transition states, the lowest-energy conformers are determined by performing calculations for the most likely structures. The thermodynamic properties for important species during the pyrolysis of PA and CoA calculated at

the CBS-QB3 level of theory are provided in Table S6. The thermodynamic properties for other species in the mechanism are derived from the group additivity estimator in Reaction Mechanism Generator (RMG), an open-source software package for automatic mechanism generation <sup>(38)</sup>. More details about the calculations can refer to the literature <sup>(39)</sup>. The weakest bonds of PA and CoA (Figure 1) are O–H bond with 345 kJ/mol and O–CH<sub>3</sub> bond with 242 kJ/mol respectively <sup>(35)</sup>. The latter is very close to guaiacol (243 kJ/mol) <sup>(19)</sup>. Similar to anisole and guaiacol, breaking the weakest O–CH<sub>3</sub> bond is expected to be the first step in CoA decomposition. In order to simulate the formation of the major quantified compounds that were experimentally observed from PA and CoA pyrolysis, the kinetic mechanisms have been constructed manually firstly based on the chemical understanding of the decomposition of compounds with similar structures. For example, the kinetic model of PA pyrolysis could refer to the thermal decomposition of phenol <sup>(14,15)</sup> and aldehydes <sup>(40)</sup>. Similarly, the kinetic model of CoA could refer to the established PA model and previous models of anisole <sup>(16–18)</sup> and guaiacol <sup>(19,20)</sup>. After that, the new proposed pathways were proved competitive (*vide infra*) and incorporated into the kinetic models. The final kinetic models have 60 and 290 reactions, as well as 31 and 69 species for PA and CoA pyrolysis respectively. These reactions contain unimolecular decomposition, isomerization, radical decomposition, H-atom abstraction and recombination. Mechanism files with the computational data can be found in the SI in CHEMKIN format.

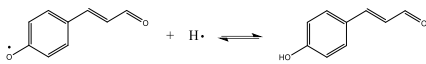
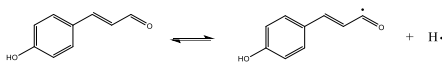
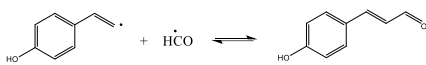

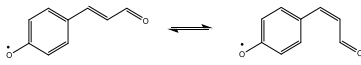
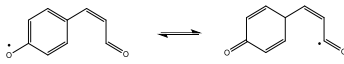

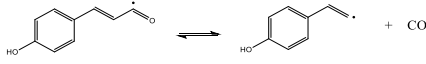
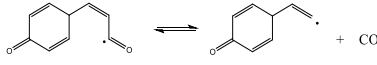
Table 1 consists of the primary reactions of PA pyrolysis. Unimolecular decomposition includes the homolysis of the weak bonds of the reactant (reactions 1-3 represented by R1-3) and the direct concerted decarbonylation (R4). The rate constants of R1-3 were estimated by analogy with the reactions of phenol <sup>(18)</sup>, n-C<sub>3</sub>H<sub>7</sub>CHO <sup>(40)</sup> and C<sub>2</sub>H<sub>3</sub>CHO <sup>(40)</sup>, respectively. R4 was assumed similar to the decarbonylation of SC<sub>3</sub>H<sub>5</sub>CHO in the AramcoMech3.0 mechanism <sup>(41)</sup>,


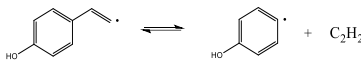


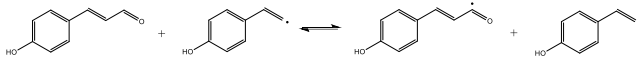
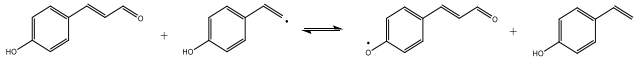
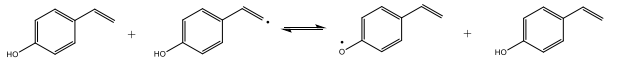
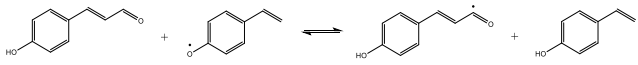
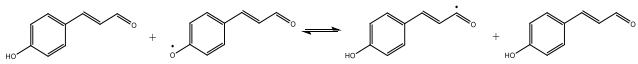

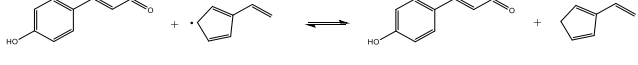
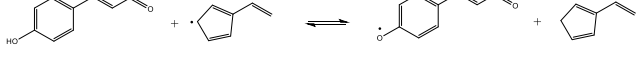
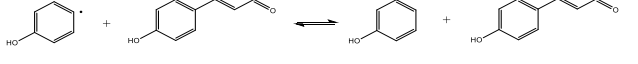
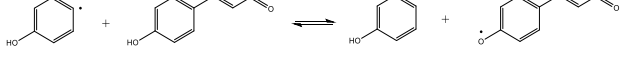


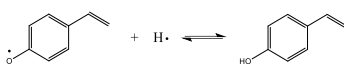
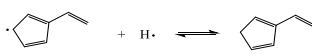
and was then adjusted within a factor of 2, which is in the range of the uncertainty limit. Trans-cis isomerization of the primary radical (R5) and the subsequent H-atom shift (R6 and R7) involve an important radical route (described in 3.1). Their rate constants were obtained from theoretical calculation at the CBS-QB3 level of theory without any tuning. Radical decomposition mainly proceeds via the removal of CO from the intermediate radicals. R8 and R9 were estimated by analogy with the reaction in radical  $\text{SC}_3\text{H}_5\dot{\text{C}}\text{O}$  <sup>(42)</sup>. R10 was supposed similar to phenoxy decomposition, and its rate constants were determined by Carstensen and Dean <sup>(43)</sup>. Approximate rate constants can also refer to the work of Pratali Maffei et al. <sup>(15)</sup>. The rate constants of R11 were derived from the kinetic database RMG <sup>(38)</sup>. For the H-atom abstraction, R12 and R13 (H atom as abstracting radical) were estimated by the analogous reactions in AramcoMech3.0 <sup>(41)</sup> and phenol <sup>(44)</sup>, respectively. H-atom abstraction initiated by vinyl-type radicals (R14-16) was written by analogous reactions (the equations are  $\dot{\text{C}}_2\text{H}_3 + \text{C}_2\text{H}_3\text{CHO} = \text{C}_2\text{H}_4 + \text{C}_2\text{H}_3\dot{\text{C}}\text{O}$ ,  $\dot{\text{C}}_2\text{H}_3 + \text{phenol} = \text{C}_2\text{H}_4 + \text{phenoxy}$ ). Their rate constants were calculated at the CBS-QB3 level. For the abstraction of phenoxy-type radicals as abstracting radicals (R17-19), the rate constants were extracted by analogy with reactions of phenoxy reacting with the aldehyde group of benzaldehyde <sup>(45)</sup>, or with the hydroxyl group of methylcatechol <sup>(19)</sup>. The H-atom abstraction of cyclopentadienyl-type radicals from the aldehyde group (R20) and OH group (R21), were assumed similar to the reaction of cyclopentadienyl with benzaldehyde and cresol respectively <sup>(46)</sup>. The H-atom abstraction by 4-hydroxyphenyl from the aldehyde group (R22) and OH group (R23) were analogous to the reactions of phenyl with benzaldehyde <sup>(46)</sup> and phenol <sup>(47)</sup>, respectively. R24 has the same kinetics as R1. The recombination of H atom and cyclopentadienyl-type radicals (R25) was supposed similar to that of H atom and cyclopentadienyl <sup>(17)</sup>. Kinetics for R26 were derived from the same reaction in AramcoMech3.0

<sup>(41)</sup>. There are other potential pathways that lead to the major products, but they have shown not to be kinetically significant (see Table S7).

Table 1. Primary mechanism for PA pyrolysis. Rate constants are in the form  $AT^n \exp(-E_a/RT)$  in cm, mol, s, and kJ units.

Reaction	A	n	E <sub>a</sub>	Ref.
<b>Unimolecular decomposition</b>				
1 	$2.00 \times 10^{14}$	0.00	0.00	(18)
2 	$2.72 \times 10^{17}$	-0.58	372.60	(40)
3 	$1.81 \times 10^{13}$	0.00	0.00	(40)
4 	$1.23 \times 10^{11}$	0.00	220.00	(41)
<b>Isomerization</b>				
5 	$4.54 \times 10^{11}$	0.25	107.19	a
6 	$1.06 \times 10^9$	1.20	136.84	a
7 	$4.70 \times 10^5$	2.00	91.37	a
<b>Radical decomposition</b>				
8 	$8.60 \times 10^{15}$	0.00	96.23	(42)
9 	$8.60 \times 10^{15}$	0.00	96.23	(42)

10		$2.67 \times 10^{72}$	-16.95	378.27	(43)
11		$8.35 \times 10^{14}$	-0.07	189.10	(38)
<b>Hydrogen abstraction</b>					
12		$1.34 \times 10^{13}$	0.00	13.81	(41)
13		$1.15 \times 10^{14}$	0.00	51.87	(44)
14		1.09	3.72	-1.83	a
15		1.11	3.88	1.90	a
16		1.11	3.88	1.90	a
17		$1.60 \times 10^5$	2.00	38.00	(45)
18		$1.60 \times 10^5$	2.00	38.00	(45)
19		$9.80 \times 10^{11}$	0.00	39.36	(19)
20		$1.30 \times 10^{11}$	0.00	48.12	(46)
21		$4.90 \times 10^{11}$	0.00	39.33	(46)
22		$1.30 \times 10^{11}$	0.00	48.15	(46)
23		$4.91 \times 10^{12}$	0.00	18.42	(47)

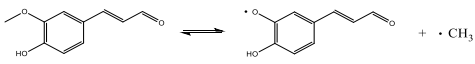
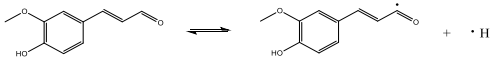
Recombination					
24		$2.00 \times 10^{14}$	0.00	00.00	(18)
25		$3.16 \times 10^{13}$	0.28	0.75	(17)
26	$\text{H}_2 \rightleftharpoons \cdot\text{H} + \cdot\text{H}$	$4.58 \times 10^{19}$	-1.40	437.10	(41)

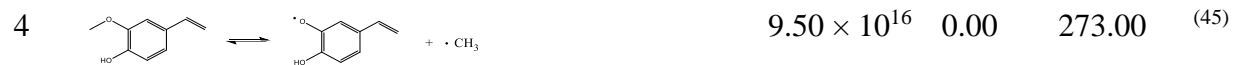
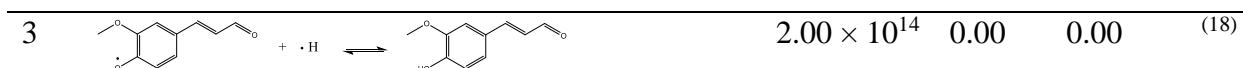
<sup>a</sup> analogous reactions calculated at CBS-QB3 level

Table 2 gives an overview of the most important reactions of CoA pyrolysis. Note that those reactions that had almost no contribution for PA consumption were also not considered in the development of the CoA model, such as the indirect CO elimination from the ring of PA after internal rearrangement of the reactant (Table S7). The reactions similar to those in the PA decomposition mechanism have been assigned the same rate constants, and will not be re-introduced here. Specifically, homolysis of the weakest O–CH<sub>3</sub> bond (R1 and R4) leading to phenoxy-type and CH<sub>3</sub> radicals was derived from the analogous reaction in guaiacol<sup>(45)</sup>. But the rate constants were reduced within a factor of 2 in this work, considering that the BDE of O–CH<sub>3</sub> bond in CoA is 3.0 kJ/mol higher than that in guaiacol<sup>(45)</sup>. This adjustment also improves the agreement with the experimental data. The H-atom shift (R5 and R6) between the two oxygen atoms of the primary radical was theoretically calculated at the CBS-QB3 level of theory. The formed para-phenoxy radical can then isomerize (R7-9) similar to that in the PA decomposition mechanism. The 2-methoxyphenoxy radical can go through the similar pathway (R10-12). The rate constants of R7-12 referred to those of analogous reactions in PA decomposition mechanism. For the primary radical formed in R1, another possible pathway directly starting from trans-cis isomerization is not competitive and is shown in Table S8. The rate constants of H-atom shift from methoxy to hydroxyl (R13 and R14) were theoretically calculated at the CBS-QB3 level of

theory. Further isomerization (R15 and R16) is similar to that in the benzaldehyde mechanism<sup>(48)</sup>. The subsequent radical decomposition via  $\beta$ -scission (R17 and R18) producing an aldehyde on the aromatic ring was theoretically calculated at the CBS-QB3 level of theory. For the decomposition of 4-vinyl-hydroxyphenoxy (R22 and R23), it can undergo two CO elimination reactions, which was estimated by analogy with a one-step simplified reaction of 2-hydroxyphenoxy leading to two CO, one H atom and C<sub>4</sub>H<sub>4</sub><sup>(45)</sup>. Note that the mechanism to benzene might be incomplete, and this estimation needs further optimization and confirmation via theoretical calculations or more detailed experiments. H-atom abstraction from the aldehyde group of the reactant by a methyl radical (R32) was calculated at the CBS-QB3 level. H-atom abstraction from the hydroxyl group (R33) was estimated by analogy with the abstraction of phenol by methyl<sup>(49)</sup>. The H-atom abstraction by H-atom from the aldehyde group (R34) and OH group (R35) were analogous to the reactions of H-atom with C<sub>2</sub>H<sub>3</sub>CHO and phenol in AramcoMech3.0<sup>(41)</sup>, respectively. Rate constants of radical recombination (R38) were estimated based on the similar reactions<sup>(50)</sup>. Kinetics for the recombination of methyl with a hydrogen or methyl radical (R39 and R40) were taken from the same reactions in the AramcoMech3.0<sup>(41)</sup>.

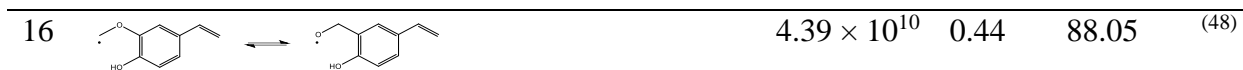
Table 2. Primary mechanism for CoA pyrolysis. Rate constants are in the form  $AT^n \exp(-E_a/RT)$  in cm, mol, s, and kJ units.

Reaction	A	n	E <sub>a</sub>	Ref.
Unimolecular decomposition				
1 	$9.50 \times 10^{16}$	0.00	273.00	(45)
2 	$2.72 \times 10^{17}$	-0.58	372.60	(40)

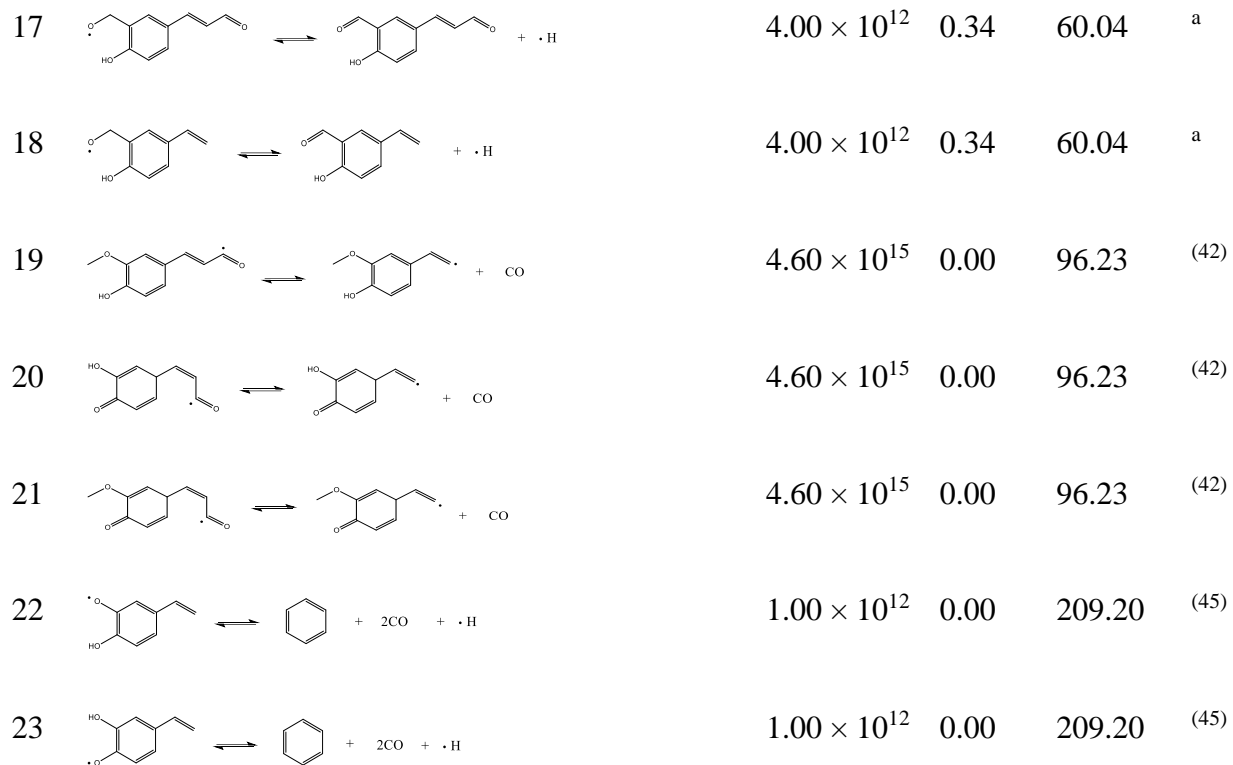


### Isomerization

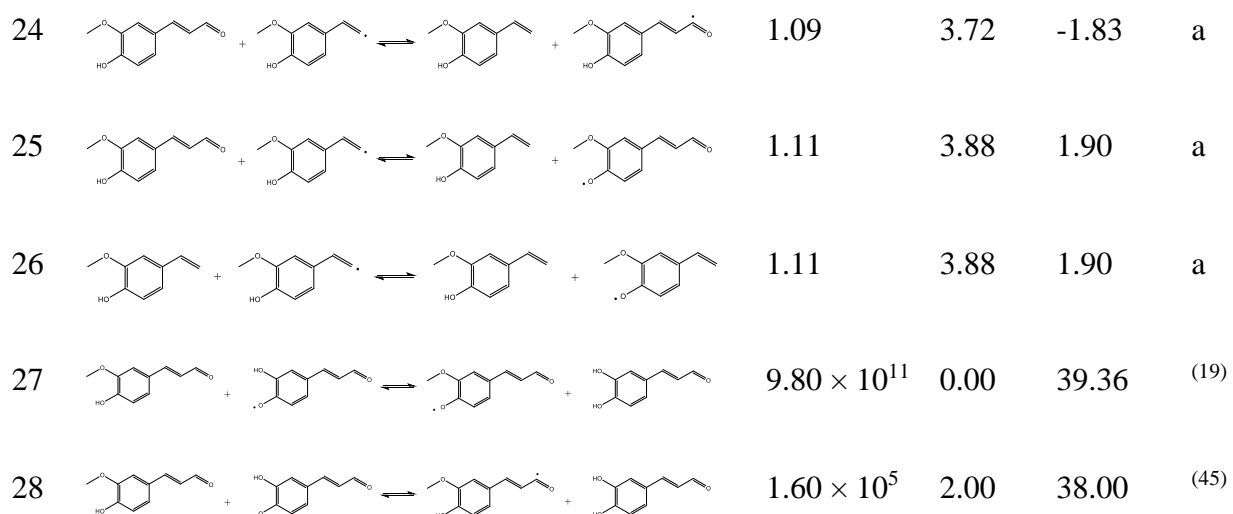




### Radical decomposition



### Hydrogen abstraction



29		$1.60 \times 10^5$	2.00	38.00	(45)
30		$1.60 \times 10^5$	2.00	38.00	(45)
31		$9.80 \times 10^{11}$	0.00	39.36	(19)
32		5.97	3.78	16.35	a
33		$1.80 \times 10^{11}$	0.00	32.23	(49)
34		$1.34 \times 10^{13}$	0.00	13.82	(41)
35		$1.15 \times 10^{14}$	0.00	51.91	(41)

### Recombination

36		$2.00 \times 10^{14}$	0.00	0.00	(18)
37		$2.00 \times 10^{14}$	0.00	0.00	(18)
38		$1.00 \times 10^{13}$	0.00	0.00	b
39	$\cdot\text{CH}_3 + \cdot\text{H} \rightleftharpoons \text{CH}_4$	$1.27 \times 10^{16}$	-0.63	1.60	(41)
40	$\cdot\text{CH}_3 + \cdot\text{CH}_3 \rightleftharpoons \text{C}_2\text{H}_6$	$2.28 \times 10^{15}$	-0.69	0.73	(41)

<sup>a</sup> analogous reactions calculated at CBS-QB3 level

<sup>b</sup> estimated

The 2<sup>nd</sup> reactor in which the thermal decomposition occurs functions as a plug flow reactor (PFR)

<sup>(51)</sup>. Reactor simulations in this work were performed using the PFR module in CHEMKIN PRO

<sup>(52)</sup> to model the micro-pyrolysis reactor based on the inlet flow compositions, measured



temperature profiles along the reactor, and reactor dimensions. The reactor model equations can be found in the SI.

### 3. Results and Discussion

#### 3.1. Potential energy surface for the proposed radical pathways

Knowing the phenoxy-type radicals chemistry is crucial for understanding the combustion/pyrolysis of lignocellulosic biomass. For the simple phenoxy radical ( $C_6H_5\dot{O}$ ), the dissociation to cyclopentadienyl and CO is well-known and considered the most important decomposition pathway at high temperatures<sup>(43)</sup>. For primary phenoxy-type radicals in PA and CoA pyrolysis (namely radical  $P(OI)$  and  $C(OI)$  in Figure 2), the decomposition pathway similar to phenoxy is shown in Figure 3, and the total barriers in this process calculated at the CBS-QB3 level are 237.7 and 267.4 kJ/mol respectively.

Figure 2a shows a new consumption pathway for the radical  $P(OI)$  in PA decomposition mechanism. The first step is the trans-cis isomerization of radical  $P(OI)$  with an energy barrier as low as 106.5 kJ/mol. Formed cis-isomer of  $P(OI)$  undergoes the internal H-atom shift through a 5-membered ring intermediate (TSp2) toward radical  $P(C3)$  with the energy barrier of 146.0 kJ/mol, followed by the release of CO to yield radical  $P(C2)$  with the energy barrier of 126.3 kJ/mol. Intermediate  $P(C2)$  converts to a much more stable radical  $V(OI)$  via internal H-atom migration (TSp4) with the energy barrier of 112.5 kJ/mol. The total barrier for CO elimination for this new pathway that was identified in the present work is 249.2 kJ/mol. In contrast, another CO release pathway of the radical  $P(OI)$ , similar to phenoxy radical ( $C_6H_5\dot{O}$ ) ring-opening to cyclopentadienyl plus CO, has a little lower barrier of 237.7 kJ/mol (Figure 3a). Nevertheless, this new pathway shows the importance of resonance. The reactants used in this work were

determined to be entirely in trans form via the GC/TOF-MS tests, considering the importance of interconversion of radicals between the trans-cis forms.

Similarly, the new consumption pathway identified in the present work for the primary radical  $C(O1)$  in the CoA decomposition mechanism is shown in Figure 2b. Radical  $C(O1)$  can first easily isomerize to form the more stable para-phenoxy radical  $C(O2)$ , then followed by the isomerization similar to the radical  $P(O1)$  in PA decomposition mechanism. The total barrier for CO release in this pathway is 218.8 kJ/mol. This value is much lower than the 267.4 kJ/mol mentioned earlier in the decomposition similar to phenoxy (Figure 3b), indicating that the proposed pathway is kinetically more favourable. Radical  $C(O1)$  could also skip the first H-shift between the two oxygen atoms and directly start the trans-cis isomerization. This pathway with a higher total barrier (232.2 kJ/mol) is shown in Figure S3. Note that the radicals similar to radical  $C(O1)$  are very abundant in the thermal decomposition of real lignin because of the abundance of weak O-CH<sub>3</sub> bond and  $\beta$ -O-4 linkages in lignin <sup>(24)</sup>.

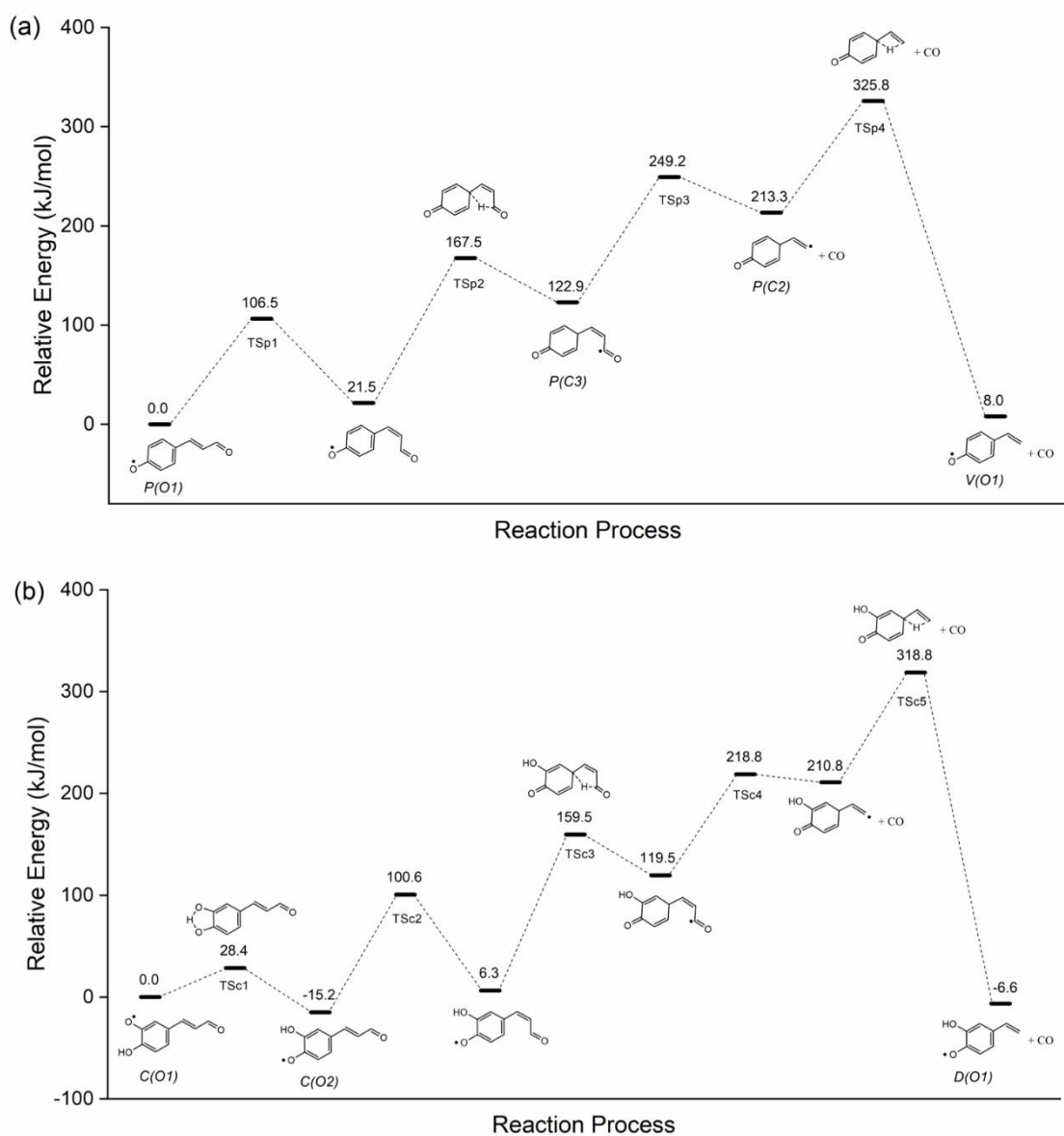


Figure 2. Potential energy surface for the proposed new pathway in (a) PA and (b) CoA pyrolysis. The values were calculated at 0 K with the CBS-QB3 level of theory.

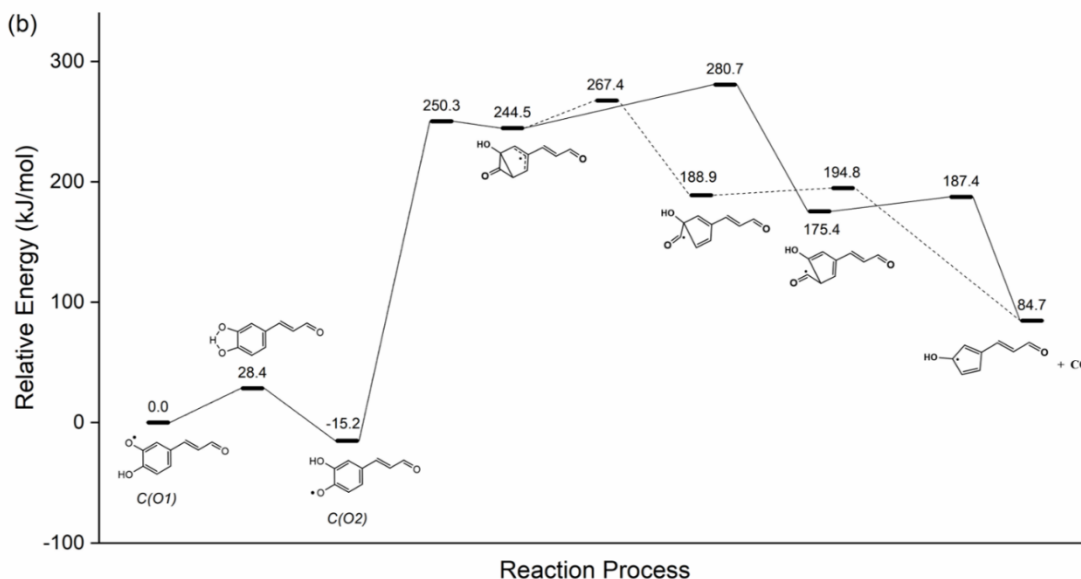
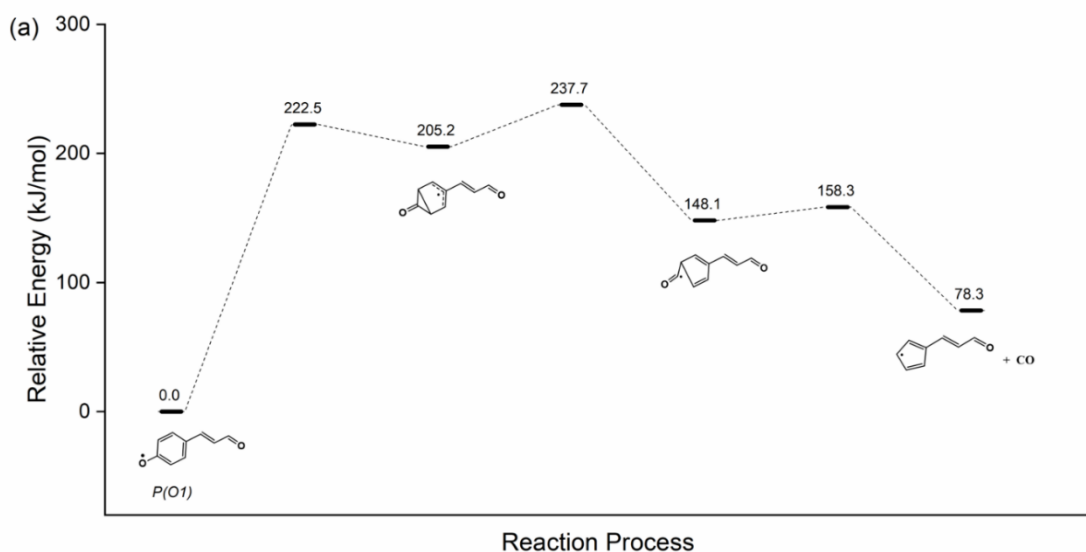


Figure 3. Potential energy surface for the decomposition pathway similar to phenoxy decomposition in the case of primary phenoxy-type radicals from (a) PA and (b) CoA pyrolysis. The values were calculated at 0 K with the CBS-QB3 level of theory.

The idea of finding a new pathway was originally to produce experimentally observed species. For the experimental results of CoA pyrolysis, 4-vinyl guaiacol is the primary aromatic product at low temperatures, but 4-vinylbenzene-1,2-diol becomes the dominant one at high temperatures. The structures are shown in Table 3 (*vide infra*). At first, we assumed that 4-vinylbenzene-1,2-

diol was formed by the further decomposition of 4-vinyl guaiacol, but this assumption was overturned by the following two facts. (1) 4-vinylbenzene-1,2-diol is extremely underestimated in the simulation if it is only produced by the further decomposition of 4-vinyl guaiacol. (2) If the above assumption was correct, namely 4-vinyl guaiacol leading to a large amount of 4-vinylbenzene-1,2-diol, CoA should also lead to a large amount of 3,4-dihydroxycinnamaldehyde. However, the mole fraction of 4-vinylbenzene-1,2-diol experimentally observed is much higher than that of 3,4-dihydroxycinnamaldehyde. Therefore, there should be other pathways producing a large amount of 4-vinylbenzene-1,2-diol at high temperatures. We searched many possible pathways and decided to adopt the one in this work based on the calculated rate coefficients.

### **3.2. Thermal decomposition of PA**

The pyrolysis of PA has been studied as a function of temperature from 873 to 1123 K. Figure 4a shows the evolution of the mole fraction of PA. PA starts to decompose at around 923 K and reaches 81% conversion at 1123 K. In total, 32 species were identified and quantified from the chromatograms (Table S9). A GC  $\times$  GC FID chromatogram at 1123 K is shown in Figure S4a. The major pyrolysis products are CO, 4-vinylphenol, vinylcyclopentadiene, phenol, C<sub>2</sub>H<sub>2</sub> and H<sub>2</sub> (displayed in Figure 4b-g), and their mole fractions increase rapidly with increasing temperature. The mole fraction of CO is a little higher than 4-vinylphenol at temperatures above 1023 K, while they have comparable mole fractions at lower temperatures. The other four major products (Figure 4d-g) appear from decomposition temperatures of 973 K and above have significantly lower prevalence than CO and 4-vinylphenol during the whole pyrolysis temperatures. Simulation results (solid lines) and experimental data (symbols) are in good agreement (Figure 4), except the slight overestimation for 4-vinyl phenol and CO, and the underestimation for the other four major products above 1073 K.

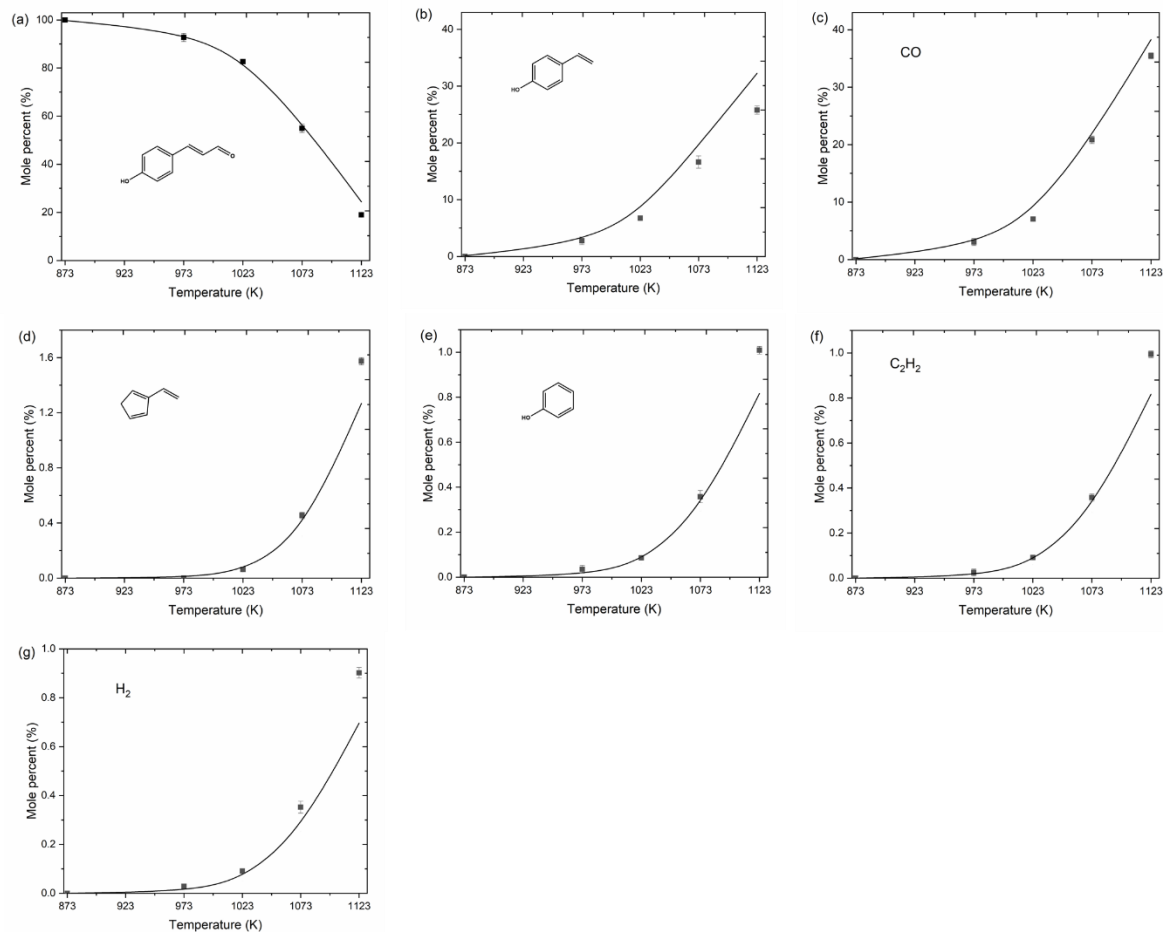


Figure 4. Evolution of mole fractions of (a) PA and (b-f) its major pyrolysis products as a function of the temperature. Symbols refer to experimental results and lines to our model.

A rate of production (ROP) analysis performed at 1123 K for PA pyrolysis is illustrated in Figure 5. This temperature was selected since its radical chemistry only becomes obvious at high temperatures. The net-rates of the reactions are shown as a percentage relative to the total consumption of PA and they are calculated using CHEMKIN PRO. The dominant thermal decomposition pathway of PA is the concerted decarbonylation reaction yielding 4-vinylphenol and CO, which accounts for 92.5% of the total PA consumption. By contrast, radical chemistry is less important. The second pathway leads to the formation of a phenoxy-type radical  $P(OI)$  via H-atom abstraction from the hydroxyl group or the direct homolytic cleavage of O–H bond,

which is responsible for 5.2% of the consumption flux. The dissociation of radical  $P(OI)$  to CO and cyclopentadienyl-type radical, similar to that of phenoxy  $C_6H_5\dot{O}$ , accounts for only 0.1% of the total consumption flux and thus is not shown in Figure 5. A more competitive pathway, as discussed in 3.1, leads to radical  $V(OI)$  and CO, which accounts for 5.0% of the consumption flux. In addition, 4-vinylphenol can partly be consumed to form radical  $V(OI)$  (2.5%). The produced radical  $V(OI)$  then decomposes to CO and the vinylcyclopentadienyl radical. The latter is resonantly stabilized and leads to several vinylcyclopentadiene isomers through H-atom abstraction or recombination with H atoms. This is reflected in the GC image figure (Figure S4a) and here 2-vinylcyclopenta-1,3-diene is selected to represent these isomers. A minor route of PA consumption is the H-atom abstraction at the  $C_\gamma$  position or homolysis of the  $C_\gamma-H$  bond leading to radical  $P(C9)$  (2.2%) which then converts to radical  $V(C2)$  and CO through decarbonylation. The radical  $V(C2)$  tends to produce  $C_2H_2$  and phenol via a  $\beta$ -scission reaction and an H-atom abstraction. In the concerted decarbonylation pathway, equal moles of CO and 4-vinylphenol are produced. The presence of the radical pathways explains why there is more CO than 4-vinylphenol at high temperatures.

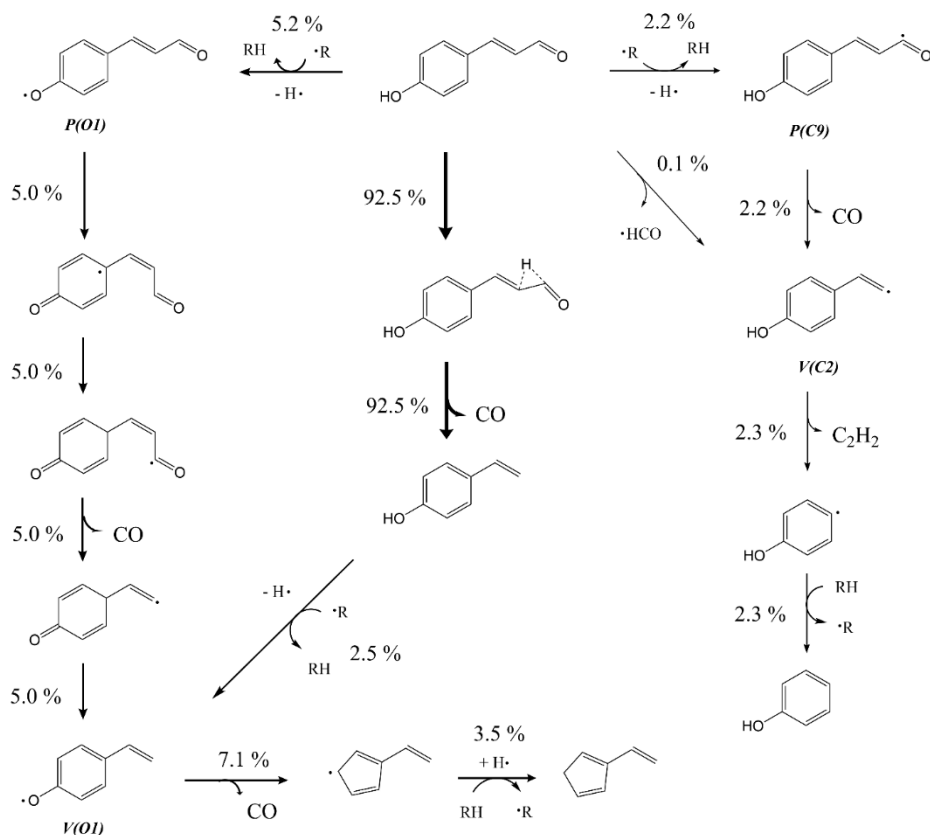


Figure 5. Rate of production analysis for PA pyrolysis at 1123 K, 3.5 atm with residence time of 0.33 s. Reaction fluxes associated with arrows are relative to the consumption of PA.

### 3.3. Thermal decomposition of CoA

Figure 6 displays the evolution of the mole fraction of CoA during gas-phase pyrolysis in the temperature range from 723 to 923 K. CoA decomposition starts at 723 K and reaches 50% conversion at around 848 K. Above 898 K, its mole fraction becomes close to zero and the conversion is almost complete. Compared with PA, the reactivity of CoA pyrolysis is much higher, as seen by the lower temperatures needed for the initial decomposition and total conversion. This is attributed to a weak O–CH<sub>3</sub> bond with a low BDE of 242 kJ/mol. CoA has a similar decomposition profile shape to that reported for anisole<sup>(16–18)</sup> and guaiacol<sup>(19,20)</sup>, two compounds similar to CoA containing a methoxy group attached to the aromatic ring.



CoA pyrolysis leads to the formation of dozens of compounds, including light products and aromatics (Table S10). A GC × GC FID chromatogram at 848 K is shown in Figure S4b. The main light products, in order of decreasing mole fraction at 848 K, are CO, C<sub>2</sub>H<sub>6</sub>, CH<sub>4</sub> and H<sub>2</sub>, and their profiles are presented in Figure 6b-e. CO and C<sub>2</sub>H<sub>6</sub> are produced in large amounts above 823 K and reach maximum mole fractions of about 52% and 12% at the highest studied temperature, respectively. The formation of CH<sub>4</sub> is usually from H-atom abstraction by methyl radicals, and its mole fraction reaches a maximum of 3.6% at 873 K. The subsequent decline corresponds to the temperature of complete conversion of CoA. At higher temperature, H-atom abstraction by methyl radicals on the products of CoA decomposition such as 4-vinylguaiacol is more difficult than on CoA, as shown in Figure 7 (*vide infra*). The methane decrease and the analogous explanation in anisole decomposition were reported by Nowakowska et al. <sup>(16)</sup>. The mole fraction of CH<sub>4</sub> is much less than C<sub>2</sub>H<sub>6</sub> above 848 K, indicating that the self-recombination occurs prior to H-atom abstraction for methyl radicals under the studied experimental conditions. The mole fraction of hydrogen reaches 0.9% at 848 K and then decreases. This is due to the decrease of H-atom formation, and the increased formation of abstracting radicals such as radical *D(OI)* above 848 K, as shown in Figure 7 (*vide infra*). Besides, minor production of ethylene and acetylene was observed. The aromatic products formed in large quantities are presented in Figure 6f-l, and their names and structures are shown in a nomenclature table (Table 3). The yield of oxygen-containing aromatic products shows a bell-shape profile with maxima around 823–873 K. However, the yield of benzene continued to increase with temperature, likely due to the breaking of C–C and C–O bonds attached to the aromatic ring of the oxygen-containing aromatic products. 4-vinyl guaiacol appears from decomposition temperatures of 723 K, the lowest temperature investigated in the present work, and shows the largest mole fraction among

aromatics below 848 K, indicating that it is produced from the primary decomposition of CoA. 2-hydroxy-5-(3-oxoprop-1-en-1-yl)benzaldehyde and 2-hydroxy-5-vinylbenzaldehyde are produced similar to the 2-hydroxybenzaldehyde formation from guaiacol through the OCH<sub>3</sub> rearrangement pathway<sup>(19,20)</sup>. They reach a maximum mole fraction of 2.5% at 848 K and 3.3% at 873 K, respectively. Above 848 K, 4-vinylbenzene-1,2-diol becomes the dominant aromatic product and reaches a maximum of 8.8% at 873 K. The mole fraction of 2-methoxy-4-propenylphenol peaks at 1.2% around 873 K, and then decreases due to the breaking of the O-CH<sub>3</sub> bond. By comparison, 3,4 dihydroxycinnamaldehyde is less important, but its maximum mole fraction peaks at lower temperature of 823 K. Lighter aromatics are produced at higher temperatures, such as benzene with a maximum mole fraction around 3.8% at 923 K. In addition, other aromatics such as styrene, ethylbenzene, 2-methyl-phenol and 2-methyl-4-vinylphenol were detected in smaller quantities.

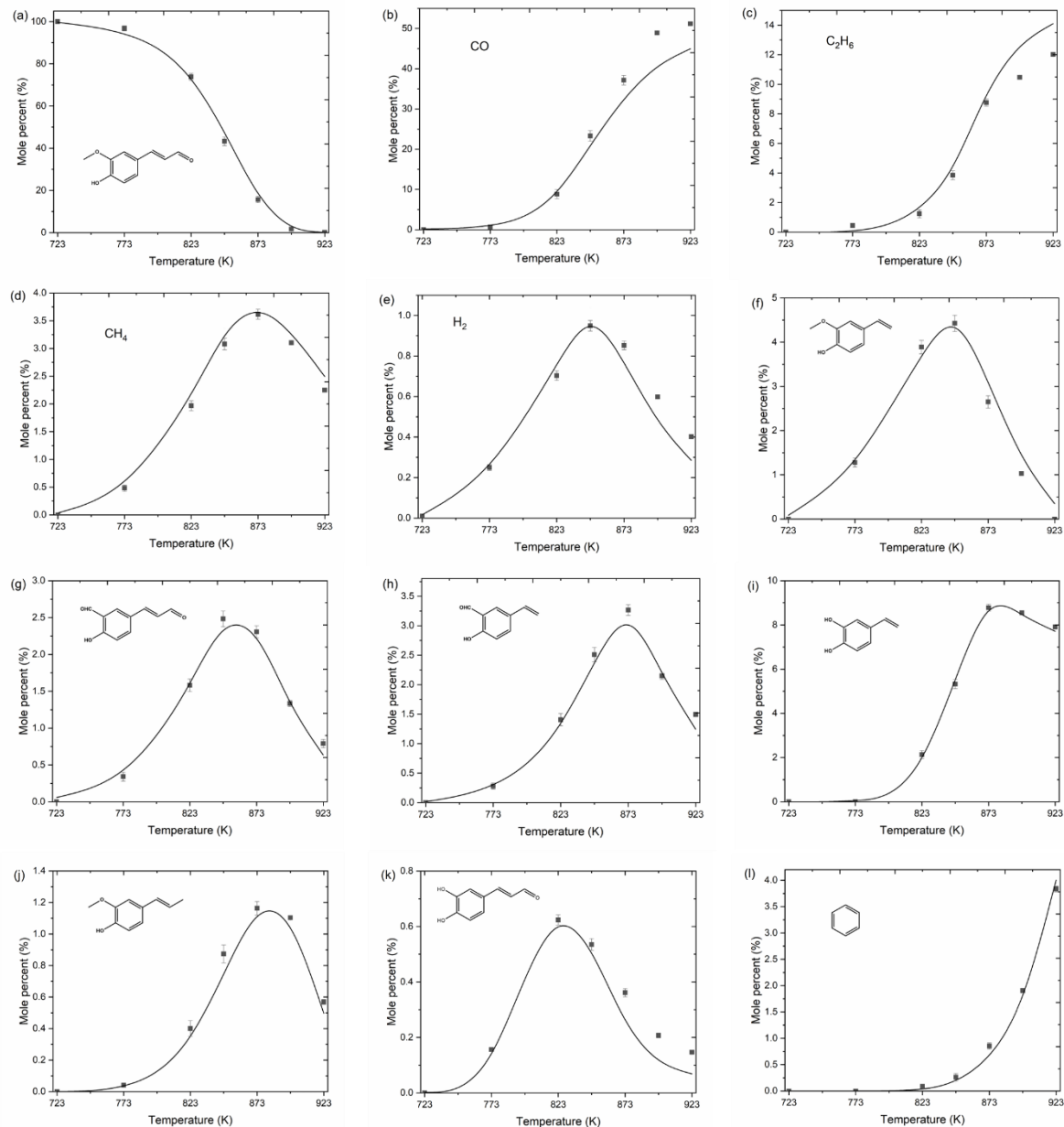
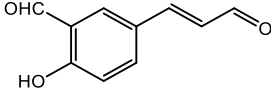
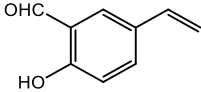
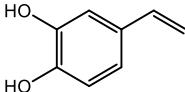
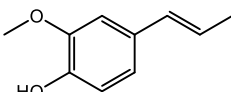
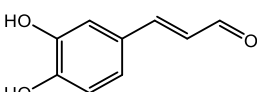
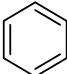


Figure 6. Evolution of mole fractions of (a) trans-CoA and (b-i) its major pyrolysis products as a function of the temperature. Symbols refer to experimental results and lines to our model.

Table 3. Nomenclature of the major aromatics derived from CoA pyrolysis.

Name	Structure
4-vinylguaiacol	

2-hydroxy-5-(3-oxoprop-1-en-1-yl)benzaldehyde	
2-hydroxy-5-vinylbenzaldehyde	
4-vinylbenzene-1,2-diol	
2-methoxy-4-propenylphenol	
3,4-dihydroxycinnamaldehyde	
Benzene	

Simulation results well predict the conversion of CoA and the formation of the major products (Figure 6). The main discrepancies between simulations and experiments appear above 848 K, with the model overestimating the mole fractions of 4-vinyl guaiacol and  $C_2H_6$ , but underestimating CO,  $H_2$  and 3,4 dihydroxycinnamaldehyde. Based on the model developed in this work, the thermal decomposition routes of CoA at 823 and 898 K are displayed in Figure 7, representing the simulated conversion of 26% and 98%, respectively. The unimolecular breaking of the O- $CH_3$  bond yielding a methyl and phenoxy-type radical  $C(OI)$  is the dominant initial pathway under these two temperatures with 45.3% and 78.8% of the consumption flux. This is in good agreement with the study of the thermal decomposition of anisole and guaiacol<sup>(18,19)</sup>. At 823 K, 4-vinyl guaiacol is the major aromatic product while at 898 K 4-vinylbenzene-1,2diol is favoured over other aromatic products. The primary radical  $C(OI)$  can easily convert to radical  $D(OI)$  and CO through the proposed pathway (bold arrows). Taking 823 K as an example, the formed radical  $D(OI)$  together with its isomer (dashed box) then leads to the formation of 4-

vinylbenzene-1,2-diol by either the recombination with H atoms (9.9%) or H-atom abstraction (5.5%), or further decomposes to benzene and CO (0.1%), similar to two consecutive decarboxylation of 2-hydroxyphenoxy radical <sup>(45)</sup>. This proposed pathway explains why a large amount of 4-vinylbenzene-1,2-diol was experimentally detected above 823 K. In contrast, the pathway of radical *C(O1)* direct converting to 3,4-dihydroxycinnamaldehyde (5.3%) by H-atom abstraction or recombination with H atoms is not competing, especially at higher temperature of 898 K (0.5%). The second pathway of CoA consumption is H-atom abstraction from the side-chain aldehyde group yielding radical *C(C9)*, which represents 31.1% of the consumption flux. After that, this radical converts to radical *T(C2)* through the ejection of CO, which then mainly forms 4-vinylguaiacol by H-atom abstraction (28.2%). Part of radical *T(C2)* leads to 2-methoxy-4-propenylphenol (2.9%) via the recombination with methyl. The further decomposition of primary product 4-vinylguaiacol has a little contribution to the formation of 4-vinylbenzene-1,2-diol (0.8%). The third pathway of CoA consumption is the H-atom abstraction from the hydroxyl group yielding radical *C(O2)*, which represents 20.6% of the consumption flux. This radical can partly convert to radical *D(O2)*, similar to the pathway with bold arrows. Radical *D(O2)* can also be derived from the consumption of 4-vinyl guaiacol (0.1%). The formed radical *D(O2)* finally yields 2-hydroxy-5-vinylbenzaldehyde (10.6%). Only 3.0% CoA is consumed by the H-atom abstraction from the methoxy group, the formed radical and the remaining radical *C(O2)* finally convert to 2-hydroxy-5-(3-oxoprop-1-en-1-yl)benzaldehyde (13.1%). This type of pathway describing the conversion of OCH<sub>3</sub> to CHO group on the aromatic ring has been reported <sup>(19,20)</sup>.

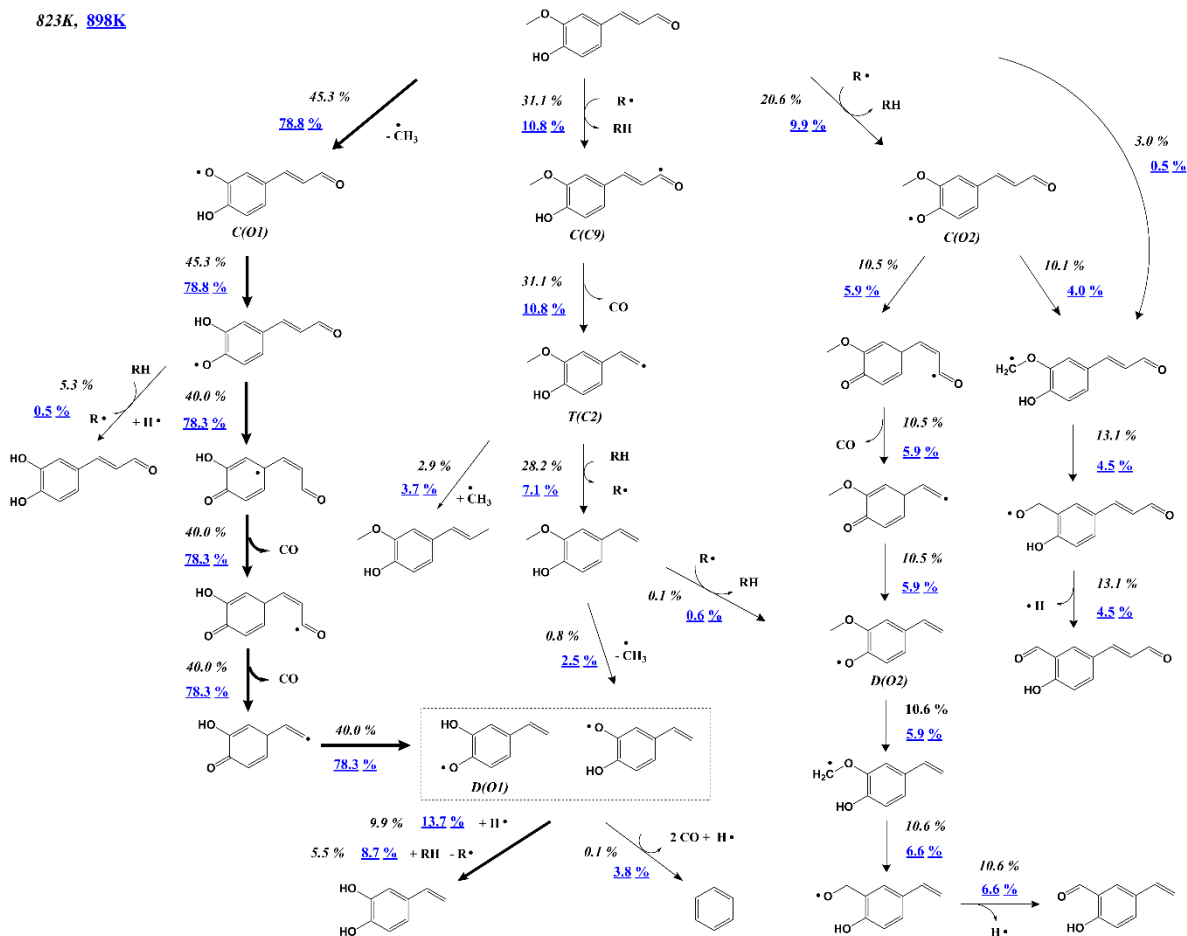


Figure 7. Rate of production analysis for CoA pyrolysis at 823 K (black) and 898 K (blue) with residence time of  $\pm 0.4$  s. Reaction fluxes associated with arrows are relative to the consumption of CoA.

The main reasons for the slightly decreased agreement between model and experimental data of the two developed kinetic models at higher temperatures are: (1) we focussed on the pathways leading to the dominating products that were experimentally detected, and (2) very heavy products with a boiling point above 723 K are not quantifiable using gas chromatography. Because we use an internal standard quantification of lighter compounds remains possible. However, it results in the fact that only 75% of the decomposition products being formed at 1123 K for PA pyrolysis can be quantified, while this increases to 75–85% at 848–923 K for CoA pyrolysis, and 91–100% at lower temperatures ( $<848$  K) (Figure S5). The missing products at the higher decomposition temperatures are primarily PAHs /coke precursors (outside the GC range)

and a minor amount of coke, which is confirmed by the black deposits seen on the quartz tube after pyrolysis (Figure S6). This is in line with reports by other researchers such as Ranzi and co-workers that lignin monomers have a strong tendency to form PAHs and coke during pyrolysis<sup>(45)</sup>. On the other hand, the underestimation of hydrogen at high temperatures in PA and CoA decomposition mechanisms should be due to the formation of PAHs / coke, which results in hydrogen released into gas phase. Considering the formation of PAHs / coke in the kinetic model is part of our future work.

## 5. Conclusions

The gas-phase pyrolysis of *p*-coumaraldehyde (PA) and coniferaldehyde (CoA) was studied for the first time. The new experimental data were gathered in a tandem reactor equipped with a comprehensive analysis section that can detect and quantify pyrolysis products with boiling points up to 823 K next to permanent gases. A newly identified consumption pathway that involves the interaction between hydroxyl and side-chains of primary phenoxy-type radicals was proposed based on calculating the potential energy surface at the CBS-QB3 level of theory. First-principles based kinetic models comprising this new pathway were developed. The models predict the experimentally observed profiles of reactants and major products well at the studied temperatures. Rate of production (ROP) analysis reveals that PA is mainly consumed at 1123 K through the concerted decarbonylation in the side-chain, whereas the proposed pathway is less important even though it is the second consumption pathway. For CoA pyrolysis, the addition of the methoxy group to the aromatic ring makes it more reactive. ROP results indicate that the consumption of CoA is dominated by the breaking of the weak O–CH<sub>3</sub> bond at 823 and 898 K to produce a methyl and a phenoxy-type radical. The latter continues to be consumed mainly through the proposed pathway, which explains why 4-vinylbenzene-1,2-diol becomes the

dominant aromatic product at higher temperatures. The insights obtained from this study can (1) provide an idea for the fate of the similar radicals with substituents and side-chains during the thermo-chemical processes of biomass, and (2) help to develop detailed kinetic mechanisms for the pyrolysis/combustion of aromatic fuels and lignin.

### Supporting Information

The following files are available free of charge.

- Kinetic models (separated files in CHEMKIN format) (Text S1), reactor model for the 2<sup>nd</sup> reactor of the micro-pyrolysis setup (Text S2), secondary mechanisms for PA and CoA pyrolysis (Text S3, Table S7 and S8), schematic diagram of the micro-pyrolyzer unit and the temperatures measured along the 2<sup>nd</sup> reactor (Figure S1), the vaporization profiles of PA and CoA in the 1<sup>st</sup> reactor (Figure S2), PES for a potential decomposition pathway of primary phenoxy-type radicals in CoA pyrolysis (Figure S3), GC × GC FID chromatograms obtained for the pyrolysis of PA at 1123 K and CoA at 848 K (Figure S4), mass balances and molar balances of C, H and O elements for the pyrolysis of PA and CoA (Figure S5), reactor (new) before and (old) after pyrolysis experiments (Figure S6), overview of the columns used in LOA GC and GC × GC (Table S1 and S2), LOA GC temperature program (Table S3), GC × GC settings for the simultaneous FID/TOF-MS analysis (Table S4), overview of the temperature conditions for the micro-pyrolyzer tests (Table S5), thermodynamic properties for important species during the pyrolysis of PA and CoA calculated at the CBS-QB3 level of theory (Table S6), the less important reactions in the mechanism of PA and CoA pyrolysis (Table S7 and S8), and products formed from PA and CoA pyrolysis (Table S9 and S10). (PDF)
- Kinetic model of *p*-coumaraldehyde pyrolysis (TXT)



- Kinetic model of coniferaldehyde pyrolysis (TXT)

## Author Information

### Corresponding Author

**Kevin M. Van Geem** - *Laboratory for Chemical Technology, Ghent University, Technologiepark 125, 9052 Zwijnaarde, Belgium;*

ORCID <http://orcid.org/0000-0003-4191-4960>;

Email: [Kevin.VanGeem@UGent.be](mailto:Kevin.VanGeem@UGent.be)

### Authors

**Liang Li** - *Laboratory for Chemical Technology, Ghent University, Technologiepark 125, 9052 Zwijnaarde, Belgium*

**Ruben Van de Vijver** - *Laboratory for Chemical Technology, Ghent University, Technologiepark 125, 9052 Zwijnaarde, Belgium*

**Andreas Eschenbacher** - *Laboratory for Chemical Technology, Ghent University, Technologiepark 125, 9052 Zwijnaarde, Belgium*

**Florence H. Vermeire** - *Laboratory for Chemical Technology, Ghent University, Technologiepark 125, 9052 Zwijnaarde, Belgium;*

ORCID <https://orcid.org/0000-0002-5607-8152>

### Notes

The authors declare no competing financial interest.

### Acknowledgments

Liang Li thanks the financial support from the Overseas Study Program of Guangzhou Elite Project. Ruben Van de Vijver acknowledges financial support from the Fund for Scientific Research Flanders (FWO) grant number 3E013419. The research leading to these results has received funding from the European Research Council under the innovation programme / ERC grant agreements n° 818607 (ERC OPTIMA). This work was carried out using the STEVIN

Supercomputer Infrastructure at Ghent University, funded by Ghent University, the Flemish Supercomputer Center (VSC), the Hercules Foundation and the Flemish Government – department EWI.

## References

1. Kostetskyy, P.; Broadbelt, L. J. Progress in Modeling of Biomass Fast Pyrolysis: A Review. *Energy and Fuels*. 2020, DOI:10.1021/acs.energyfuels.0c02295.
2. Fahmy, T. Y. A.; Fahmy, Y.; Mobarak, F.; El-Sakhawy, M.; Abou-Zeid, R. E. Biomass Pyrolysis: Past, Present, and Future. *Environ. Dev. Sustain.* **2020**, 22 (1), 17–32, DOI:10.1007/s10668-018-0200-5.
3. Seljak, T.; Buffi, M.; Valera-Medina, A.; Chong, C. T.; Chiaramonti, D.; Kutrašnik, T. Bioliquids and Their Use in Power Generation – A Technology Review. *Renew. Sustain. Energy Rev.* **2020**, 129, 109930, DOI:10.1016/j.rser.2020.109930.
4. Brown, R. C. Heterodoxy in Fast Pyrolysis of Biomass. *Energy and Fuels*. 2021, DOI:10.1021/acs.energyfuels.0c03512.
5. Yanez, A. J.; Natarajan, P.; Li, W.; Mabon, R.; Broadbelt, L. J. Coupled Structural and Kinetic Model of Lignin Fast Pyrolysis. *Energy and Fuels* **2018**, 32 (2), DOI:10.1021/acs.energyfuels.7b03311.
6. Pinheiro Pires, A. P.; Arauzo, J.; Fonts, I.; Domine, M. E.; Fernández Arroyo, A.; Garcia-Perez, M. E.; Montoya, J.; Chejne, F.; Pfromm, P.; Garcia-Perez, M. Challenges and Opportunities for Bio-Oil Refining: A Review. *Energy and Fuels*. 2019, DOI:10.1021/acs.energyfuels.9b00039.
7. Vanholme, R.; Demedts, B.; Morreel, K.; Ralph, J.; Boerjan, W. Lignin Biosynthesis and Structure. *Plant Physiol.* **2010**, 153 (3), 895–905, DOI:10.1104/pp.110.155119.
8. Kawamoto, H.; Horigoshi, S.; Saka, S. Pyrolysis Reactions of Various Lignin Model Dimers. *J. Wood Sci.* **2007**, 53 (2), 168–174, DOI:10.1007/s10086-006-0834-z.
9. Kim, K. H.; Bai, X.; Brown, R. C. Pyrolysis Mechanisms of Methoxy Substituted A-O-4 Lignin Dimeric Model Compounds and Detection of Free Radicals Using Electron Paramagnetic Resonance Analysis. *J. Anal. Appl. Pyrolysis* **2014**, 110 (1), 254–263, DOI:10.1016/j.jaap.2014.09.008.
10. Wang, S.; Ru, B.; Dai, G.; Shi, Z.; Zhou, J.; Luo, Z.; Ni, M.; Cen, K. Mechanism Study on the Pyrolysis of a Synthetic  $\beta$ -O-4 Dimer as Lignin Model Compound. *Proc. Combust. Inst.* **2017**, 36 (2), 2225–2233, DOI:10.1016/j.proci.2016.07.129.
11. Huang, Y.; Liu, S.; Zhang, J.; Syed-Hassan, S. S. A.; Hu, X.; Sun, H.; Zhu, X.; Zhou, J.; Zhang, S.; Zhang, H. Volatile–Char Interactions during Biomass Pyrolysis: Cleavage of C–C Bond in a  $\beta$ -5 Lignin Model Dimer by Amino-Modified Graphitized Carbon Nanotube. *Bioresour. Technol.* **2020**, 307, 123192, DOI:10.1016/j.biortech.2020.123192.
12. Jarvis, M. W.; Daily, J. W.; Carstensen, H. H.; Dean, A. M.; Sharma, S.; Dayton, D. C.; Robichaud, D. J.; Nimlos, M. R. Direct Detection of Products from the Pyrolysis of 2-

- Phenethyl Phenyl Ether. *J. Phys. Chem. A* **2011**, *115* (4), 428–438, DOI:10.1021/jp1076356.
13. Khachatryan, L.; Adoukpe, J.; Dellinger, B. Formation of Phenoxy and Cyclopentadienyl Radicals from the Gas-Phase Pyrolysis of Phenol. *J. Phys. Chem. A* **2008**, *112* (3), 481–487, DOI:10.1021/jp073999m.
  14. Scheer, A. M.; Mukarakate, C.; Robichaud, D. J.; Nimlos, M. R.; Carstensen, H. H.; Barney Ellison, G. Unimolecular Thermal Decomposition of Phenol and d 5-Phenol: Direct Observation of Cyclopentadiene Formation via Cyclohexadienone. *J. Chem. Phys.* **2012**, *136* (4), 044309, DOI:10.1063/1.3675902.
  15. Pratali Maffei, L.; Pelucchi, M.; Faravelli, T.; Cavallotti, C. Theoretical Study of Sensitive Reactions in Phenol Decomposition. *React. Chem. Eng.* **2020**, *5* (3), DOI:10.1039/c9re00418a.
  16. Nowakowska, M.; Herbinet, O.; Dufour, A.; Glaude, P. A. Detailed Kinetic Study of Anisole Pyrolysis and Oxidation to Understand Tar Formation during Biomass Combustion and Gasification. *Combust. Flame* **2014**, *161* (6), 1474–1488, DOI:10.1016/j.combustflame.2013.11.024.
  17. Wagnon, S. W.; Thion, S.; Nilsson, E. J. K.; Mehl, M.; Serinyel, Z.; Zhang, K.; Dagaut, P.; Konnov, A. A.; Dayma, G.; Pitz, W. J. Experimental and Modeling Studies of a Biofuel Surrogate Compound: Laminar Burning Velocities and Jet-Stirred Reactor Measurements of Anisole. *Combust. Flame* **2018**, *189*, 325–336, DOI:10.1016/j.combustflame.2017.10.020.
  18. Yuan, W.; Li, T.; Li, Y.; Zeng, M.; Zhang, Y.; Zou, J.; Cao, C.; Li, W.; Yang, J.; Qi, F. Experimental and Kinetic Modeling Investigation on Anisole Pyrolysis: Implications on Phenoxy and Cyclopentadienyl Chemistry. *Combust. Flame* **2019**, *201*, 187–199, DOI:10.1016/j.combustflame.2018.12.028.
  19. Nowakowska, M.; Herbinet, O.; Dufour, A.; Glaude, P. A. Kinetic Study of the Pyrolysis and Oxidation of Guaiacol. *J. Phys. Chem. A* **2018**, *122* (39), 7894–7909, DOI:10.1021/acs.jpca.8b06301.
  20. Nguyen, T. T. P.; Mai, T. V. T.; Huynh, L. K. Detailed Kinetic Modeling of Thermal Decomposition of Guaiacol – A Model Compound for Biomass Lignin. *Biomass and Bioenergy* **2018**, *112*, 45–60, DOI:10.1016/j.biombioe.2018.02.006.
  21. Gonzalez-Quiroga, A.; Van Geem, K. M.; Marin, G. B. Towards First-Principles Based Kinetic Modeling of Biomass Fast Pyrolysis. *Biomass Convers. Biorefinery* **2017**, *7* (3), 305–317, DOI:10.1007/s13399-017-0251-0.
  22. Dellon, L. D.; Sung, C. Y.; Robichaud, D. J.; Broadbelt, L. J. 110th Anniversary: Microkinetic Modeling of the Vapor Phase Upgrading of Biomass-Derived Oxygenates. *Ind. Eng. Chem. Res.* **2019**, *58* (33), 15173–15189, DOI:10.1021/acs.iecr.9b03242.
  23. Asatryan, R.; Bennadji, H.; Bozzelli, J. W.; Ruckenstein, E.; Khachatryan, L. Molecular Products and Fundamentally Based Reaction Pathways in the Gas-Phase Pyrolysis of the Lignin Model Compound p-Coumaryl Alcohol. *J. Phys. Chem. A* **2017**, *121* (18), 3352–3371, DOI:10.1021/acs.jpca.7b01656.

24. Kawamoto, H. Lignin Pyrolysis Reactions. *J. Wood Sci.* **2017**, *63* (2), 117–132, DOI:10.1007/s10086-016-1606-z.
25. Khachatryan, L.; Xu, M. X.; Wu, A. J.; Pechagin, M.; Asatryan, R. Radicals and Molecular Products from the Gas-Phase Pyrolysis of Lignin Model Compounds. Cinnamyl Alcohol. *J. Anal. Appl. Pyrolysis* **2016**, *121*, 75–83, DOI:10.1016/j.jaap.2016.07.004.
26. Fan, L.; Zhang, Y.; Liu, S.; Zhou, N.; Chen, P.; Cheng, Y.; Addy, M.; Lu, Q.; Omar, M. M.; Liu, Y.; Wang, Y.; Dai, L.; Anderson, E.; Peng, P.; Lei, H.; Ruan, R. Bio-Oil from Fast Pyrolysis of Lignin: Effects of Process and Upgrading Parameters. *Bioresour. Technol.* **2017**, *241*, 1118–1126, DOI:10.1016/j.biortech.2017.05.129.
27. Liu, C.; Ye, L.; Yuan, W.; Zhang, Y.; Zou, J.; Yang, J.; Wang, Y.; Qi, F.; Zhou, Z. Investigation on Pyrolysis Mechanism of Guaiacol as Lignin Model Compound at Atmospheric Pressure. *Fuel* **2018**, *232*, 632–638, DOI:10.1016/j.fuel.2018.05.162.
28. Harman-Ware, A. E.; Crocker, M.; Kaur, A. P.; Meier, M. S.; Kato, D.; Lynn, B. Pyrolysis-GC/MS of Sinapyl and Coniferyl Alcohol. *J. Anal. Appl. Pyrolysis* **2013**, *99*, 161–169, DOI:10.1016/j.jaap.2012.10.001.
29. Kotake, T.; Kawamoto, H.; Saka, S. Pyrolysis Reactions of Coniferyl Alcohol as a Model of the Primary Structure Formed during Lignin Pyrolysis. *J. Anal. Appl. Pyrolysis* **2013**, *104*, 573–584, DOI:10.1016/j.jaap.2013.05.011.
30. Arias, M. E.; Polvillo, O.; Rodríguez, J.; Hernández, M.; González-Pérez, J. A.; González-Vila, F. J. Thermal Transformations of Pine Wood Components under Pyrolysis/Gas Chromatography/Mass Spectrometry Conditions. *J. Anal. Appl. Pyrolysis* **2006**, *77* (1), 63–67, DOI:10.1016/j.jaap.2005.12.013.
31. Van Acker, R.; Déjardin, A.; Desmet, S.; Hoengenaert, L.; Vanholme, R.; Morreel, K.; Laurans, F.; Kim, H.; Santoro, N.; Foster, C.; Goeminne, G.; Légée, F.; Lapiere, C.; Pilate, G.; Ralph, J.; Boerjan, W. Different Routes for Conifer- and Sinapaldehyde and Higher Saccharification upon Deficiency in the Dehydrogenase CAD1. *Plant Physiol.* **2017**, *175* (3), 1018–1039, DOI:10.1104/pp.17.00834.
32. Toraman, H. E.; Vanholme, R.; Borén, E.; Vanwongerghem, Y.; Djokic, M. R.; Yildiz, G.; Ronsse, F.; Prins, W.; Boerjan, W.; Van Geem, K. M.; Marin, G. B. Potential of Genetically Engineered Hybrid Poplar for Pyrolytic Production of Bio-Based Phenolic Compounds. *Bioresour. Technol.* **2016**, *207*, 229–236, DOI:10.1016/j.biortech.2016.02.022.
33. Toraman, H. E.; Abrahamsson, V.; Vanholme, R.; Van Acker, R.; Ronsse, F.; Pilate, G.; Boerjan, W.; Van Geem, K. M.; Marin, G. B. Application of Py-GC/MS Coupled with PARAFAC2 and PLS-DA to Study Fast Pyrolysis of Genetically Engineered Poplars. *J. Anal. Appl. Pyrolysis* **2018**, *129*, 101–111, DOI:10.1016/j.jaap.2017.11.022.
34. SriBala, G.; Toraman, H. E.; Symoens, S.; Déjardin, A.; Pilate, G.; Boerjan, W.; Ronsse, F.; Van Geem, K. M.; Marin, G. B. Analytical Py-GC/MS of Genetically Modified Poplar for the Increased Production of Bio-Aromatics. *Comput. Struct. Biotechnol. J.* **2019**, *17*, 599–610, DOI:10.1016/j.csbj.2019.04.007.
35. Li, L.; Van De Vijver, R.; Eschenbacher, A.; Dogu, O.; Van Geem, K. M. Primary Thermal Decomposition Pathways of Hydroxycinnamaldehydes. *Energy and Fuels* **2021**,

35 (15), 12216–12226, DOI:10.1021/acs.energyfuels.1c01662.

36. Schofield, K. The Enigmatic Mechanism of the Flame Ionization Detector: Its Overlooked Implications for Fossil Fuel Combustion Modeling. *Prog. Energy Combust. Sci.* **2008**, *34* (3), 330–350, DOI:10.1016/j.pecs.2007.08.001.
37. Frisch, M. J.; Trucks, G. W.; Schlegel, H. B.; Scuseria, G. E.; Robb, M. A.; Cheeseman, J. R.; Scalmani, G.; Barone, V.; Petersson, G. A.; Nakatsuji, H.; Li, X. Gaussian 16 Rev. C.01. Wallingford, CT. 2016.
38. Gao, C. W.; Allen, J. W.; Green, W. H.; West, R. H. Reaction Mechanism Generator: Automatic Construction of Chemical Kinetic Mechanisms. *Comput. Phys. Commun.* **2016**, *203*, DOI:10.1016/j.cpc.2016.02.013.
39. Vermeire, F. H.; Carstensen, H. H.; Herbinet, O.; Battin-Leclerc, F.; Marin, G. B.; Van Geem, K. M. Experimental and Modeling Study of the Pyrolysis and Combustion of Dimethoxymethane. *Combust. Flame* **2018**, *190*, 270–283, DOI:10.1016/j.combustflame.2017.12.001.
40. Pelucchi, M.; Somers, K. P.; Yasunaga, K.; Burke, U.; Frassoldati, A.; Ranzi, E.; Curran, H. J.; Faravelli, T. An Experimental and Kinetic Modeling Study of the Pyrolysis and Oxidation of N-C3C5 Aldehydes in Shock Tubes. *Combust. Flame* **2015**, *162* (2), 265–286, DOI:10.1016/j.combustflame.2014.07.027.
41. Zhou, C. W.; Li, Y.; Burke, U.; Banyon, C.; Somers, K. P.; Ding, S.; Khan, S.; Hargis, J. W.; Sikes, T.; Mathieu, O.; Petersen, E. L.; AlAbbad, M.; Farooq, A.; Pan, Y.; Zhang, Y.; Huang, Z.; Lopez, J.; Loparo, Z.; Vasu, S. S.; Curran, H. J. An Experimental and Chemical Kinetic Modeling Study of 1,3-Butadiene Combustion: Ignition Delay Time and Laminar Flame Speed Measurements. *Combust. Flame* **2018**, *197*, 423–438, DOI:10.1016/j.combustflame.2018.08.006.
42. Bourque, G.; Healy, D.; Curran, H.; Zinner, C.; Kalitan, D.; de Vries, J.; Aul, C.; Petersen, E. Ignition and Flame Speed Kinetics of Two Natural Gas Blends with High Levels of Heavier Hydrocarbons. *J. Eng. Gas Turbines Power* **2010**, *132* (2), 1–16, DOI:10.1115/1.3124665.
43. Carstensen, H. H.; Dean, A. M. A Quantitative Kinetic Analysis of CO Elimination from Phenoxy Radicals. In *International Journal of Chemical Kinetics*; 2012; Vol. 44, pp 75–89, DOI:10.1002/kin.20622.
44. He, Y. Z.; Mallard, W. G.; Tsang, W. Kinetics of Hydrogen and Hydroxyl Radical Attack on Phenol at High Temperatures. *J. Phys. Chem.* **1988**, *92* (8), 2196–2201, DOI:10.1021/j100319a023.
45. Pelucchi, M.; Cavallotti, C.; Cuoci, A.; Faravelli, T.; Frassoldati, A.; Ranzi, E. Detailed Kinetics of Substituted Phenolic Species in Pyrolysis Bio-Oils. *React. Chem. Eng.* **2019**, *4* (3), 490–506, DOI:10.1039/c8re00198g.
46. Bounaceur, R.; Da Costa, I.; Fournet, R.; Billaud, F.; Battin-Leclerc, F. Experimental and Modeling Study of the Oxidation of Toluene. *Int. J. Chem. Kinet.* **2005**, *37* (1), 25–49, DOI:10.1002/kin.20047.
47. Wang, H.; You, X.; Joshi, A. V.; Davis, S. G.; Laskin, A.; Egolfopoulos, F.; Law, C. K.

USC Mech Version II. High-Temperature Combustion Reaction Model of H<sub>2</sub>/CO/C<sub>1</sub>-C<sub>4</sub> Compounds. *Combust. Kinet. Lab. Univ. South. California, Los Angeles, CA*, accessed Aug 2007, 2, 96.

48. Silva, G. Da; Bozzelli, J. W. Benzoxyl Radical Decomposition Kinetics: Formation of Benzaldehyde + H, Phenyl + CH<sub>2</sub>O, and Benzene + HCO. *J. Phys. Chem. A* **2009**, *113* (25), 6979–6986, DOI:10.1021/jp902458d.
49. Da Costa, I.; Fournet, R.; Billaud, F.; Battin-Leclerc, F. Experimental and Modeling Study of the Oxidation of Benzene. *Int. J. Chem. Kinet.* **2003**, *35* (10), 503–524, DOI:10.1002/kin.10148.
50. Allara, D. L.; Shaw, R. A Compilation of Kinetic Parameters for the Thermal Degradation of N-Alkane Molecules. *J. Phys. Chem. Ref. Data* **1982**, *9* (3), 523–560, DOI:10.1063/1.555623.
51. De Ras, K.; Kusenbergh, M.; Vanhove, G.; Fenard, Y.; Eschenbacher, A.; Varghese, R. J.; Aerssens, J.; Van de Vijver, R.; Tran, L. S.; Thybaut, J. W.; Van Geem, K. M. A Detailed Experimental and Kinetic Modeling Study on Pyrolysis and Oxidation of Oxymethylene Ether-2 (OME-2). *Combust. Flame* **2022**, *238*, 111914, DOI:10.1016/j.combustflame.2021.111914.
52. Sieradzka, M.; Rajca, P.; Zajemska, M.; Mlonka-Mędrala, A.; Magdziarz, A. Prediction of Gaseous Products from Refuse Derived Fuel Pyrolysis Using Chemical Modelling Software - Ansys Chemkin-Pro. *J. Clean. Prod.* **2020**, *248*, 119277, DOI:10.1016/j.jclepro.2019.119277.

## TOC Graphic

